Egypt. J. Chem. **Vol. 68**, No. 4, pp.123 – 133 (2025)

Egyptian Journal of Chemistry

http://ejchem.journals.ekb.eg/

Ferrite nanostructures as promising candidates for voltammetric monitoring of the tumor marker vanillylmandelic acid

Hassan A.M. Hendawy[1], and Elmorsy Khaled [2]

[1]*Egyptian Drug Authority, Giza 12622, Egypt*

[2] *Applied Organic Chemistry Department, National Research Centre, El Bohouth St., Dokki, 12622 Giza, Egypt*

Abstract

The fabrication and electroanalytical futures of a novel disposable planner sensor integrated with zinc ferrite/multi-walled carbon nanotubes (ZnFR/MWCNTs) nanocomposite was introduced for selective quantification of the tumor marker vanillylmandelic acid (VMA) for early detection of neuroblastoma. The ZnFR/MWCNTs composite showed efficient electrocatalytic activity towards oxidation of VMA molecule with two distinct anodic peaks at 0.69 and 0.865 V following a diffusion-controlled reaction mechanism. Linear calibration graphs were illustrated covering the VMA concentration ranged from 0.11 to 2.74 µmol L^{-1} with a limit of detection value 0.03 µmol L^{-1} which is below the VMA concentration in the biological sample. The peak resolution between the VMA and those for homovanillic acid (HVA), uric acid (UA), and dopamine (DA) encourages the application of the disposable sensors for submicromolar assay of VMA in urine samples and fast diagnosis of neuroblastoma. The VMA oxidation mechanism was also presented based on theoretical molecular orbital studies.

Keywords: Vanillylmandelic acid; Submicromolar voltammetric assay; Zinc ferrite nanocomposite; Biological analysis; Oxidation mechanism; Neuroblastoma diagnosis

1. Introduction

Neuroblastoma, with a wide range of symptoms, arises from primitive sympathetic ganglion cells which is derived from the perimordial neural crest in infancy [1-4]. Monitoring of the major cationic catecholamine metabolites, namely vanillylmandelic acid (VMA) and homovanillic acid (HVA), in the infant urine samples offers a rapid efficient screening tool for diagnoses of neuroblastoma. High levels of catecholamine metabolites may indicate neuroblastoma tumors [5], carcinoid, and pheochromocytoma [6, 7]. Monitoring the VMA/HVA ratio in the newborn urine samples represents an early diagnosis of Menkes disease [8, 9].

Both VMA and HVA have similar molecular structure except the existence of an alcohol group attached to the aromatic ring in VMA molecule. The common analytical techniques for monitoring of catecholamines and their metabolites were reviewed [10], where the chromatographic separation methods accompanied by electrochemical detector are usually recommended [11-13]. Moreover, TLC [14], GC [15-16], HPTLC [17], immunochemical [18, 19], spectrophotometric [20], in addition to capillary electrophortic techniques were also reported [5, 21, 22].

The accurate, reliable, fast screening and early diagnosis of tumor markers are crucial requirements for a successful medical treatment of cancer [23]. The spectrometric and chromatographic techniques are complicated with tedious sample pretreatment steps operating high-cost instruments operated with well-trained personnel. These limitations obstacle the successful application of chromatographic techniques for the analysis of large samples in adequate analysis time. Contrary, the electroanalytical approaches are recommended as an accurate, selective, fast, and cheaper analytical tool for monitoring biologically and pharmaceutically active compounds with the possibility of miniaturization and commercialization [24-27].

Monitoring of the catecholamine metabolites by the electrochemical sensors was recently reviewed [28]. Basically, the carbon-based working electrodes including the traditional glassy carbon [13], carbon fiber [30], carbon paste [31-34], and screen-printed carbon sensors [35, 36] were the most common. Unmodified sensors showed significant drawbacks based on their limited sensitivity and selectivity with the possibility of overlapping of the oxidation peaks of the electroactive species present in the sample solution. Therefore, it is not possible to distinguish or recognize the electroactive species producing

*Corresponding author e-mail: elmorsykhaled@yahoo.com., Elmorsy Khaled
Receive Date: 29 July 2024, Revise Date: 31 August 2024, Accept Date: 01 September 2024
DOI: 10.21608/ejchem.2024.308170.10098

signals at nearby potentials or having similar function groups. Tailor-made or modified electrochemical sensors were encouraged for enhancing of the performance of the electroanalytical approach. Various electrode modifiers were selected for voltammetric monitoring VMA including carbon nanomaterials [37, 38], organic dyes [39, 40], Troeger's Base [41], leucine [42], surfactant [43], ferrite [44] or zirconia nanostructures [45].

Sol-gel chemical techniques were recommended as simple and cost-effective approaches for the synthesis of different mixed oxides avoiding limitations of the conventional way. Sol-gel methods are usually based on the preparation of the target metal oxides as a colloidal suspension, which is next transformed to the gel form through dehydration. Calcination of the produced gel form yields the metal oxide in the nano size scale [46-49]. The present study aimed to synthesize of zinc and copper doped ferrite nanocomposites with their successful applications as electrode modifier for fast submicromolar voltammetric screening of the tumor marker VMA in biological samples without a recorded interference of HVA, uric acid or dopamine.

2. Experimental

2.1. Chemicals and reagents

The screen-printed sensors were fabricated using homemade printing ink based on graphite powder (Aldrich, 1-2 µm) and the nail polish solution as binder. The stock VMA and HVA solutions were prepared by dissolving the standard homovanillic and vanillylmandelic acid samples (99%, Sigma-Aldrich) in distilled water. Analytical grade metal nitrate salts (Analar), were applied for synthesis of ferrite nanostructures including; $Fe(NO_3)_3.9H_2O$, $Cu(NO_3)_2{\cdot}3H_2O$ and $Zn(NO_3)_2.6H_2O$. Carbonaceous nanomaterials including multiwall carbon nanotubes (MWCNTs) and reduced graphene oxide (rG) were purchased from Sigma-Aldrich. The universal BR buffer solution (4×10^{-2} mol L^{-1}) was used as supporting electrolyte and the appropriate pH value was adjusted with NaOH solution. Potassium ferricyanide (FCN, Analar) was applied as a standard redox probe. Standard biological samples were obtained by VACSERA, Giza, Egypt.

2.2. Synthesis of zinc and copper ferrite nanostructures

The ferrite nanostructures doped with zinc and copper metals with the nominal composition ($Zn_{0.95}$ $Cu_{0.05}$ Fe_2O_4) were synthesized as described in details elsewhere [44]. The metal nitrate salts were co-precipitated by dissolving a definite stoichiometric ratio of the metal salt in distilled water under vigorous stirring for 1h. Citric acid (1:1 molar ratio to the metal ion concentration) was added, followed by addition of 10 mL ethylene glycol as a polymerization agent forming a uniform gel. The reaction medium was autoclaved in Teflon-lined autoclave for 5 h at 300 ^oC then cooled down to the room temperature to collect the ferrite nanostructures. The ferrite nanostructure was washed with ethanol, and deionized water then dried for 3h at 105 °C.

2.3. Working electrode and measuring device

Metrohm 797 VA workstation (Metrohm, Switzerland) was used for the voltammetric measurements connected with the measuring cell composed of fabricated printed sensors as an active working electrode, Pt wire as an auxiliary electrode, and Ag/AgCl reference electrode. The homemade conductive printing ink was formulated by mixing 0.6 g of commercial nail polish solution with 0.5 g graphite powder under continuous stirring and sonication for 30 min. The result homogeneous printing ink was printed onto the transparent PVC sheet through a stainless-steel mish (200µm thickness) as printed strips (5×35 mm), and cured at 50 ^oC for 2 h. After complete drying, the printed sensors were covered with a protective layer of nail polish solution leaving a circular working area of 3 mm diameter. The working electrodes surface was integrated by drop-castings of three successive 10 µL aliquots of the nanocomposite suspension solution in DMF (3 mg ZnFR and 3 mg MWCNTs in 1.0 mL DMF) onto the circular working area.

2.4. Analytical procedures

Known ascending increments of the stock VMA solution were added to the measuring cell containing 15 mL the supporting electrolyte at pH 2. After each addition, the differential pulse voltammograms (DPVs) was recorded at the following optimized electroanalytical parameters: pulse width 100 ms, pulse height 50 mV, pulse time 12 ms voltage step 6 mV and scan rate 0.05 V s^{-1}. Calibration graphs were illustrated by plotting the current values against the corresponding VMA concentration in the micromole range. The linearity parameters such as the standard deviation of intercept (SD) and the slope of the linear line (S) were estimated to calculate LOD value (3.3 SD/S) and LOQ value (10 SD/S) [50].

2.4. Analysis of VMA commercial and biological samples

The standard urine samples were fortified with known VMA concentrations, vortexed well, and mixed with methanol (1:3 ratios) to remove the sample protein. The VMA content in the fortified urine sample was assayed using the ZnFR/MWCNTs/SPCE following the recommended procedures.

2.5. Molecular orbital calculations (MOC)

The theoretical molecular orbital calculation studies were executed applying Gaussian 09 suite software [51] to explain the tentative oxidation mechanism of the VMA molecule at the electrode surface.

3. Results and discussion

3.1. Electrochemical behaviour of VMA molecule

At the blank screen-printed carbon electrode, VMA exhibited two distinct anodic oxidation peaks at 0.725 and 0.905 V corresponding to the formation of o-quinone and vanillin ending to the formation of multiple components (**Fig. 1**). Two DPV peaks were recorded at 0.687 and 0.877 V with approximately double sensitivity compared with the CV measurements.

Modification of the electrode matrix with ferrite nanostructures doped with different metal oxides showed enhanced the sensor performance regarding their sensitivity and selectivity towards the target analyte [52-54]. A noticeable shifting of the peak potential towards the cathodic direction indicates the electrocatalytic activity of the ferrite nanostructures against the electrooxidation of VMA at the electrode surface with a possible interaction between the FRNPs and VMA molecule and a

recorded enhancement of the electron transfer process compared with the unmodified electrode surface. Moreover, ZnFR showed higher peak current compared with CuFR and will be selected in the further studies **(Fig. 1)**.

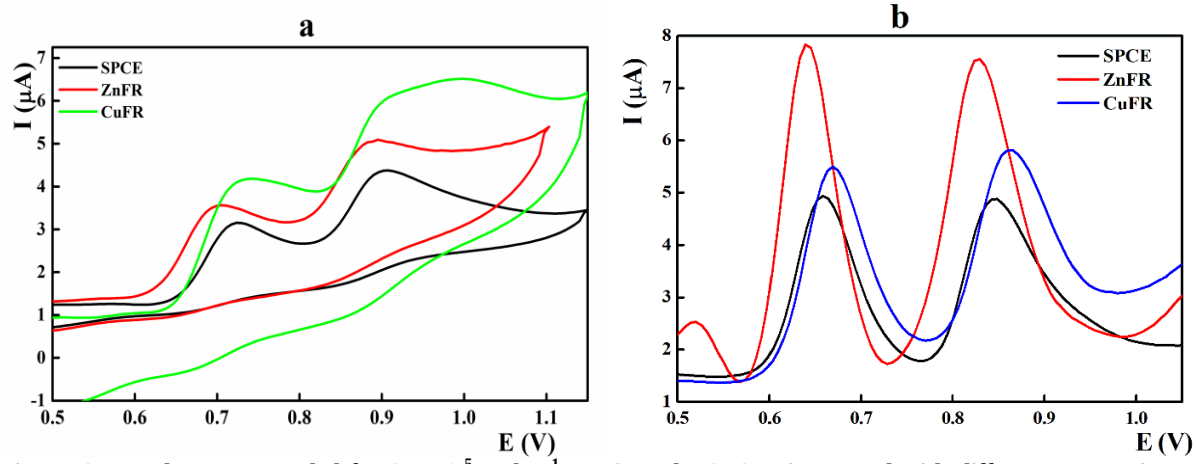

Fig. 1: CVs and DPVs recorded for 2.4×10^{-5} mol L^{-1} VMA at the SPCEs integrated with different FRNPs in BR buffer pH at 2.0 and scan rate 0.050 Vs^{-1}.

Next, the selected ferrite nanostructure **(ZnFR)** solution in DMF solution was mixed with either MWCNTs or rG forming a nanocomposite structure **(Fig. 2)**. The electrochemical behaviour of the ZnFRNPs or carbonaceous nanomaterials-based sensors was investigated in FCN solution as a proper redox probe (**Fig. 2a**). At the bare SPCE, a pair of anodic and cathodic redox peaks was recorded at 0.300 and 0.130 V. Gradual improvement of the peak current was reported upon modification with the aforementioned nanostructures and the ZnFR/MWCNTs composite showed highest peak current (about 10 folds compared with the unmodified SPCEs) with the cathodic shifting of the peak potential by about 0.050 V. The improvement of the peak current can be referred the increased effective surface area of the ZnFR/MWCNTs which promotes the electron transfer rate at the electrode surface.

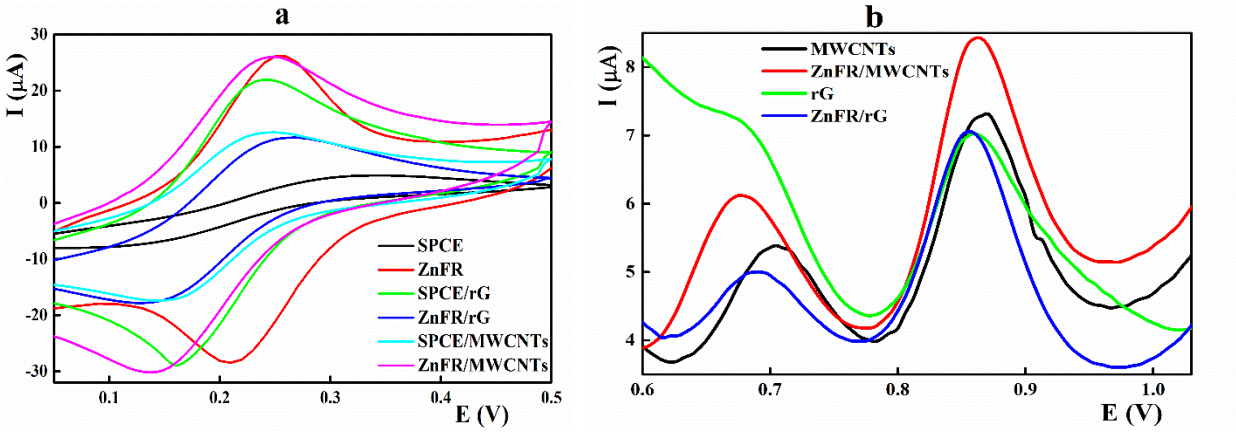

Fig. 2: a) CVs recorded in 5.0×10^{-3} mol L^{-1} $Fe(CN)_6^{3-/4-}$ solution at different ZnFR nanocomposites based sensors; b) DPVs recorded in the presence of 2.4×10^{-5} mol L^{-1} VMA in BR buffer pH 2.0 with scan rate 0.05 Vs^{-1}.

In addition to electrochemical behaviour in FCN solution, the electrode performance was evaluated against VMA molecule (**Fig. 2b**). Among the tested nanostructures, ZnFR/MWCNTs were the most proper. The oxidation peak at the rG-modified electrode was broad with a limited peak current.

3.2. Effect of pH

VMA molecule showed two p*K*a values of 3.42 related to the dissociation of the carboxylic group and 9.91 corresponding to the phenolic group [55], therefore, its electrochemical oxidation will be controlled by the pH value of the supporting electrolyte [56]. The cyclic voltammograms for VMA were monitored on bare SPCEs and ZnFR/MWCNTs based sensors at various pH values ranged from 2 to 7 (**Fig. 3, 4**). At the SPCEs, VMA showed irreversible cyclic voltammograms with oxidation potential shifted to more negative values at higher pH values due to the participation of proton in the electrode process [56]. Illustrating the peak potential against the pH values **(Fig. 3b)** showed a linear relationship (E(v)=1.0944 - 0.0654 [pH], r^2=0.9981) with Nernstian slope value indicating the involvement of an equal electrons and protons in the electrooxidation of VMA molecule. The highest recorded peak current was reported at pH 3.0 which is near to the pKa value of the VMA molecule.

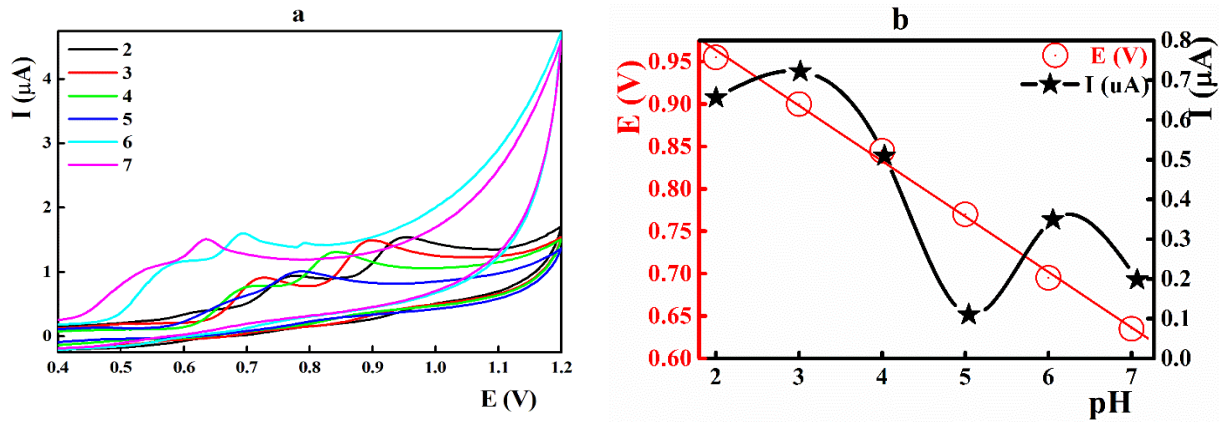

Fig. 3: a) CVs recorded at different pH values in the presence of 2.4×10^{-5} mol L^{-1} VMA at the bare SPCE, b) the recorded peak current and potential against the pH value.

Modification of the electrode surface with ZnFR/MWCNTs nanocomposite enhanced the peak current and maintained the peak performance over a wide pH range based on the possible interaction between the ferrite nanostructure and VMA molecule (**Fig. 4**). Near Nernstian slope value was reported over the pH range from 3 to 6 (*E* (v)=1.0157 - 0.0516 [pH], r^2=0.9938) with the highest peak current at pH 4.

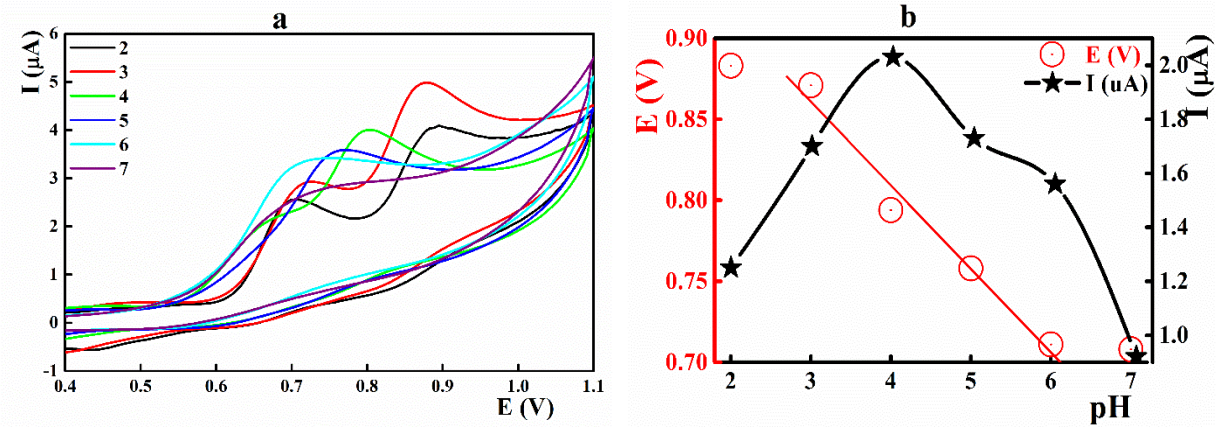

Fig. 4: a) CVs recorded at different pH values in the presence of 2.4×10^{-5} molL^{-1} VMA at the ZnFR/MWCNTs/SPCE, and b) the peak current and potential versus the pH value.

3.3. Oxidation at different scan rate values

Studying the cyclic voltammograms at different scan rate values explain the electrooxidation behavior of the target analyte at the ZnFRNPs/MWCNTs/SPCE surface and estimates the electrons transferred in the electrooxidation process [56-58]. The voltammetric behavior of the VMA molecule was monitored at both blank and ferrite-based electrodes applying a wide scan rate range (**Fig. 5, 6)**. Shifting of the oxidation potential to more positive values with enhancement the peak current at evaluated scan rate values indicated the irreversibility of the oxidation process (**Fig. 5a**). For both oxidation peaks, the peak current linearly correlated against the square root values of the scan rate (r^2=0.99177 and 0.99994 for the first and second peaks, respectively) sustaining the irreversibility of the oxidation reaction (**Fig. 5b**). The logarithmic value of the recorded peak current followed a linear relationship against the logarithmic value of the scan rate (log $I_{(\mu A)}$ =0.5661 + 0.3460 *[log (v)]*, r^2=0.9975 for the first peak and log $I_{(\mu A)}$ =0.8012 + 0.4508 *[log (v)]*, r^2=0.9999 for the second peak) with slope values typical for the diffusion control processes (**Fig. 5c**).

The oxidation potential values were shifted to the anodic direction following a linear dependence on the applied scan rate values [$E_{(V)}$*=0.7815 + 0.0461±0.0011 log (v), r=0.9957,* for the first peak and $E_{(V)}$ *=0.9431 + 0.0290±0.0002 log (v), r=0.9946* for the second peak **Fig. 5d**]. Following the Laviron equation for irreversible electrode reactions, the number of electrons involved in the oxidation process was calculated to be 1.61 and 2.56 electrons for the first and second peaks, respectively [59]:

$$Ep = E^0 + \left(\frac{2.303RT}{\propto nF}\right) log\left(\frac{RTK^0}{\propto nF}\right) + \frac{2.303RT}{\propto nF} logv$$

Where: R) ideal gas constant, T) temperature, α) electron transfer coefficient, *n*) total number of electrons transferred, and F) Faraday constant.

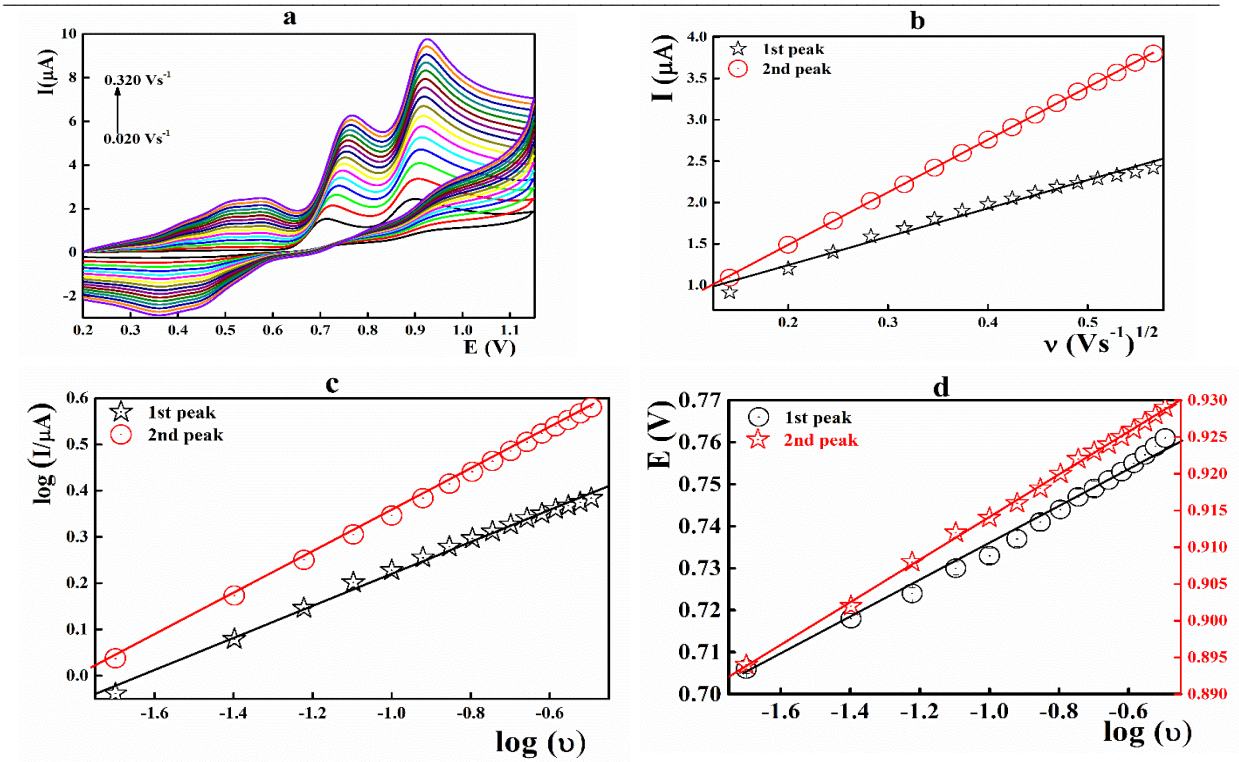

Fig. 5: a) CVs recorded for 2.4×10^{-5} mol L^{-1} VMA at the bare SPCEs applying different scan rate values; b) the peak height against the square root of the scan rate; c) the logarithmic value of the peak current against the logarithmic value of the scan rate, and d) the peak potential against the logarithmic value of the scan rate.

Parallel to the voltammetric behaviour of VMA at the bare SPCE, the effect of the scan rate was explored at the ZnFR/MWCNTs integrated sensor within the sweep rate values ranged from 0.025 to 0.325 V s^{-1} (**Fig. 6a**).

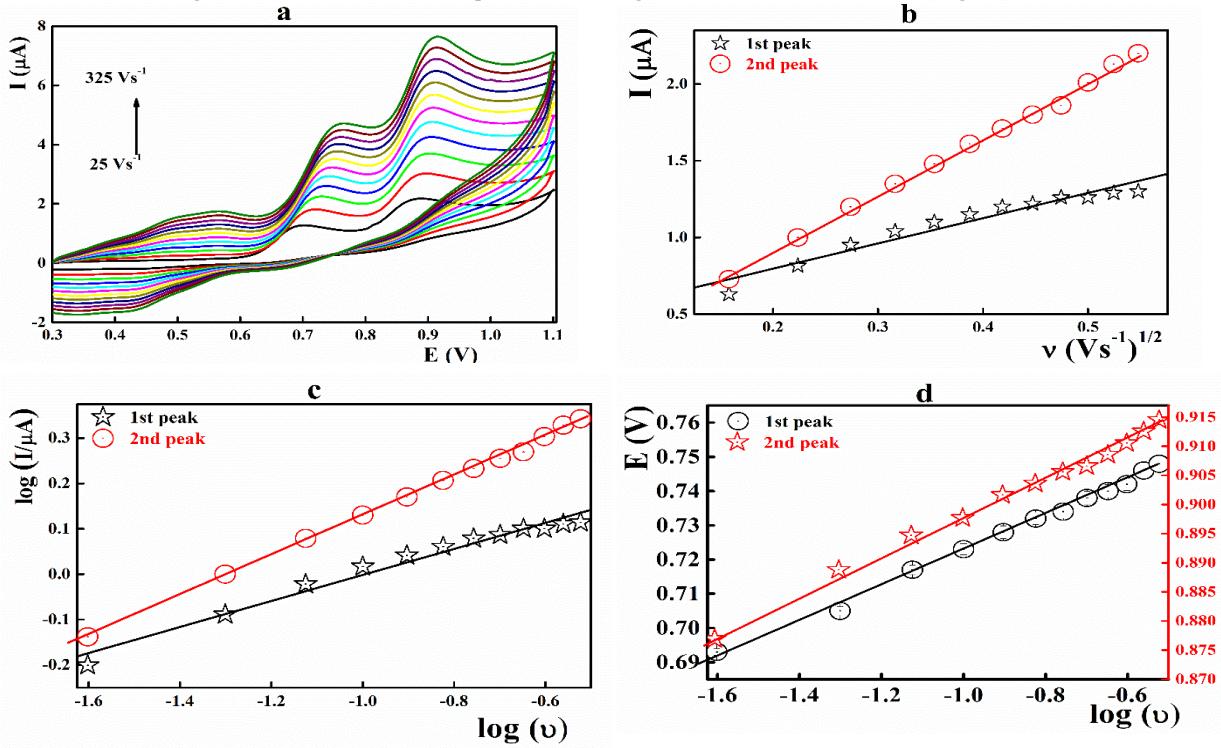

Fig. 6: a) CVs recorded for 2.4×10^{-5} mol L^{-1} VMA at ZnFR/MWCNTs/SPCEs applying different scan rate values; b) the peak height against the square root of the scan rate; c) the logarithmic value of the peak current against the logarithmic value of the scan rate, and d) the peak potential against the logarithmic value of the scan rate.

Figure 6b illustrated linear relations between the peak currents against the square root of frequency (r^2=0.9705 and 0.9987 for both peaks) indicating the irreversibility of the oxidation process. The linear relation between the logarithmic values of peak current versus the logarithmic value of the scan rate revealed similar slope values (0.28695 and 0.43722, for the first and second peak respectively) confirming the diffusion mechanism of the VMA molecule at the electrode surface (**Fig. 6c**). The peak potential values were linear against logarithmic value of the scan rate ([$E_{(V)}$ *=0.7737* + 0.05111±*0.0009 log (v), r=0.9981*, for the first peak and $E_{(V)}$ *=0.9314 + 0.0333±0.0008 log (v), r=0.9974* for the second peak **Fig. 6d**] indicating the transfer of 1.45 and 2.23 similar to that of the bare electrode.

Eventually, to support the tentative oxidation mechanism of VMA molecule, the Chembio-office-17 program was applied. Thus, the tentative oxidation mechanism of the VMA involved the participation of 4 electrons and 3 protons as confirmed by the effect of the pH and scan rate results **(Scheme 1 and Table 1)**. The voltammetric oxidation of enantiomeric VMA molecule at pH 2 showcases a fascinating interplay between pH, chirality, and electrochemical behaviour. At this acidic pH value, two distinct oxidation peaks at 0.687 and 0.877 V indicate a two-step process. The initial oxidation likely involves the chiral hydroxyl group on the VMA molecule. Due to the presence of two enantiomers, these hydroxyl groups can be oriented differently in space, potentially leading to slightly different environments and oxidation potentials, which explain the appearance of two peaks. This suggested mechanism agrees with those postulated in references [42].

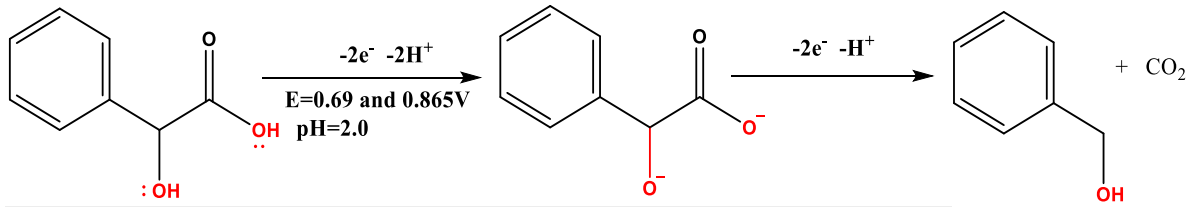

Scheme 1: Tentative electrooxidation mechanism of VMA at ZnFR/MWCNTs/SPCE surface

Table 1: Computed molecular orbital calculations of VMA molecule

Atom	Atom Type (MM2)	Mulliken Charges (Mopac Interface)	Atom Type (MMFF94)	Charge (MMFF94)	Charge (Huckel)
C(1)	C Carbonyl	0.614934	CARBOXYLIC ACID OR ESTER CARBONYL CARBON	0.659	0.594565
C(2)	C Alkane	0.043512	ALKYL CARBON, SP3	0.4845	0.151396
O(3)	O Alcohol	-0.5314	ALCOHOL OR ETHER OXYGEN	-0.68	-0.3731
C(4)	C Alkene	-0.09413	AROMATIC CARBON, E. G. IN BENZENE, PYRIDIN	-0.1435	0.07655
C(5)	C Alkene	-0.18207	AROMATIC CARBON, E. G. IN BENZENE, PYRIDIN	-0.15	-0.05201
C(6)	C Alkene	-0.20069	AROMATIC CARBON, E. G. IN BENZENE, PYRIDIN	-0.15	-0.02152
C(7)	C Alkene	-0.18642	AROMATIC CARBON, E. G. IN BENZENE, PYRIDIN	-0.15	-0.04564
C(8)	C Alkene	-0.19958	AROMATIC CARBON, E. G. IN BENZENE, PYRIDIN	-0.15	-0.02281
C(9)	C Alkene	-0.17782	AROMATIC CARBON, E. G. IN BENZENE, PYRIDIN	-0.15	-0.04943
O(10)	O Carbonyl	-0.50078	CARBONYL OXYGEN IN ACIDS AND ESTERS	-0.57	-0.62402
O(11)	O Carboxyl	-0.61596	ESTER OR CARBOXYLIC ACID -O-	-0.65	-0.16524
H(12)	H	0.241041	H ATTACHED TO C	0	0.016006
H(13)	H Alcohol	0.355306	HYDROXYL HYDROGEN IN ALCOHOLS	0.4	0.201223
H(14)	H	0.214231	H ATTACHED TO C	0.15	0.020822
H(15)	H	0.206686	H ATTACHED TO C	0.15	0.020723
H(16)	H	0.203545	H ATTACHED TO C	0.15	0.020648
H(17)	H	0.206184	H ATTACHED TO C	0.15	0.020825
H(18)	H	0.21083	H ATTACHED TO C	0.15	0.018951
H(19)	H Carboxyl	0.392584	HYDROXYL HYDROGEN IN CARBOXYLIC ACIDS	0.5	0.212053

3.4. Sensor validation

At the optimized measuring parameters, the fabricated sensors were validated by spiking successive aliquots of the stock VMA solution to the buffer solution covering a final VMA concentration ranged from 0.11 to 2.74 µ mol L^{-1}. After each addition, the corresponding DPVs were recorded and the peak current was plotted against the VMA concentration (**Fig. 7, Table 2**). High degree of linearity with low standard deviation values were recorded within the studied VMA concentration range indicating the applicability of the proposed sensor for voltammetric determination of VMA. It is noteworthy to mention that, monitoring of the oxidation process at the second peak offers better sensitivity indicated by the LOD and LOQ values reaching 0.03 and 0.11 µmolL^{-1}, respectively.

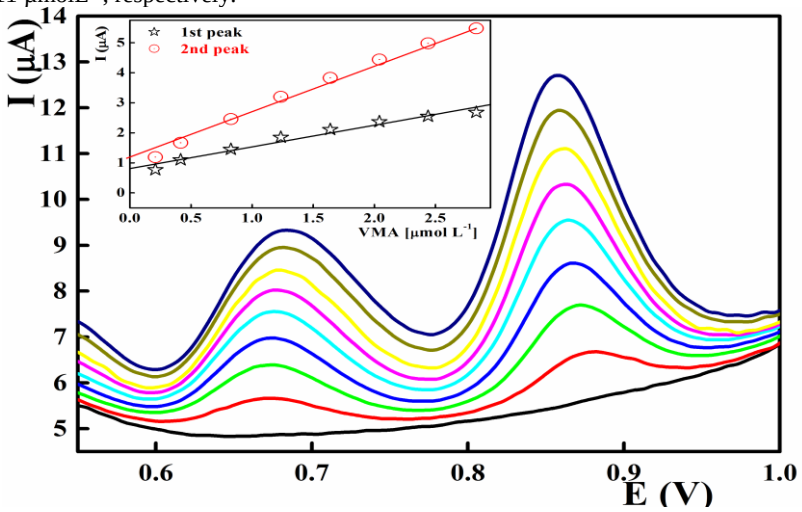

Fig. 7: Differential pulse voltammetric determination of VMA at ZnFR/MWCNTs/SPCE electrode in BR buffer at pH 2.0.

Table 2: Validation and electroanalytical futures of VMA sensors integrated with ferrite nanocomposite

Parameters	Value *	
	1st peak	2nd peak
Oxidation potential (V)	0.690	0.865
Measuring pH value	2	
Concentration range (µ mol L^{-1})	0.163- 2.83	0.11-2.74
Slope (µA µ mol L^{-1})	0.77	1.67
SD_{slope} (µA µ mol L^{-1})	0.01	0.02
Intercept (µA cm^{-2})	0.67	1.06
$SD_{intercept}$ (µA cm^{-2})	0.02	0.03
R square	1.0	1.0
RSD %	1.09	1.00
LOQ (µ mol L^{-1})	0.05	0.03
LOD (µ mol L^{-1})	0.16	0.11

*Average of five experiments

Due to the solid nature of the ZnFR/MWCNTs/SPCEs, the introduced sensors showed a prolonged shelf lifetime when stored at 4°C. The sensor performance was recorded within a storage period of 6 months. The printed sensors showed a stable and reproducible voltammetric peaks within the first three months (97.25±2.9% of the original peak current for the freshly fabricated sensor), followed by decreasing the peak height to 94.69±2.2% and 89.00±3.4% after 4 and 6 months of storage, respectively. The measuring reproducibility was tested by performing 7 successive DPVs under the optimum measuring conditions in the presence of 1.0 µ mol L^{-1} VMA at the same electrode surface. The introduced sensors showed high measurement reproducibility with a low standard deviation of 2.18%.

The performance of the presented sensor was compared with the previous VMA approaches as tabulated in Table 3. Improved sensitivity with the possibility of miniaturization and simple fabrication protocols, with long operational lifetime, offered valuable promising futures of the ZnFR/MWCNTs/SPCEs compared with the reported VMA sensors.

Table 3: Voltammetric approaches for determination of vanillylmandelic acid

Modification/working electrode	pH	Method	LOD (µ mol)	Ref.
Carbon paste electrode (CPE)	BR pH 2.0	DPV	0.4	34
Screen-printed electrode	BR pH 3.0	DPV	0.4	36
MWCNTs-Pt/GCE	PB pH 7.0	DPV	0.173	37
GCE	PB pH 3.0	DPV	0.4	40
zirconia	BR pH 4	DPV	0.273	45
Surfactants	9.5	DPV	0.02	60
ZnFR/MWCNTs	BR pH 2.0	DPV	0.03	Present study

3.5. Selectivity of the method

As previously mentioned VMA and HVA molecules showed similar structures and differ only through the presence of an alcohol group R to the aromatic ring on the VMA molecule. HVA and VMA showed an overlapped oxidation peaks at about 0.697 and 0.675 V with a specific peak for the VMA molecule at 0.865 V (**Fig. 8**). Performing the voltammetric measurements at 0.865 V allows specific and sensitive voltammetric measurements of VMA without a noticeable interference from HVA molecule.

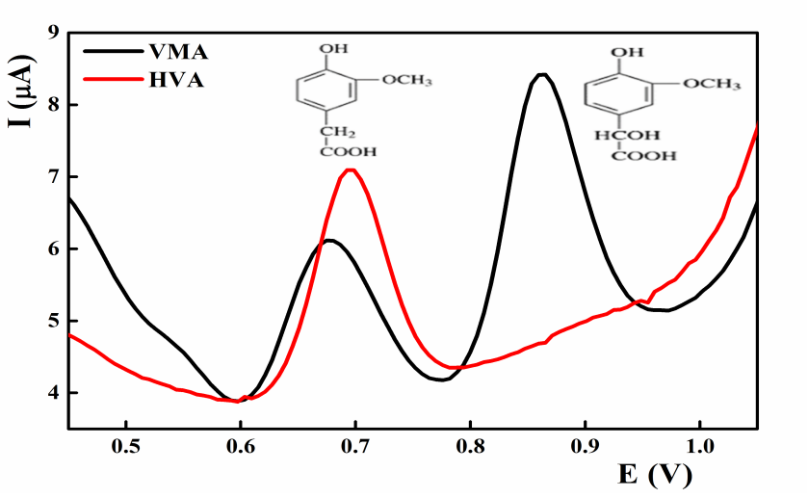

Fig. 8: Differential pulse voltammograms of 2.0×10^{-6} mol L^{-1} VMA in the presence of 3.0×10^{-6} mol L^{-1} HVA at ZnFR/MWCNTs electrode. The pH value was 2.0 and the scan rate was 0.05 V.

Dopamine (DA) and uric acid (UA) coexist at high concentrations in the urine samples which may interfere with the electrochemical monitoring of VMA. Integration of the electrode matrix with ZnFR/MWCNTs ferrite nanocomposite enhanced the resolution between the oxidation peak of UA (at 0.41 V), DA at (0.22V) and the for VMA molecules at 0.865 V.

3.6. Analysis of samples

The normal urinary VMA level ranged from 4 to 35 μmol L^{-1}, therefore the ZnFR/MWCNTs sensors with the improved sensitivity and selectivity can be encouraged as an efficient analytical tool for monitoring VMA in the urine sample without a reported interference from the species that commonly present in the urine sample such as AD, UA or other catecholamine metabolite. To verify the possible applicability of the proposed sensor, VMA content in either urine or authentic samples were monitored with the fabricated ZnFR/MWCNTs sensors. High quantitation recoveries with low RDS values were reported indicating the applicability of the fabricated sensors for monitoring of VMA in biological samples (**Table 4**).

Table 4: Assay of VMA in biological fluids at ZnFR/MWCNTs/SPCE at pH 2.0

Sample	Taken (μmol L^{-1})	Found (μmol L^{-1})	Residuals (%)	Recovery (%)
Authentic	**0.2**	**0.201**	**-0.50**	**100.50**
	0.75	**0.76**	**-1.33**	**101.33**
	1.2	**1.18**	**1.67**	**98.33**
	1.5	**1.52**	**-1.33**	**101.33**
Mean				**100.38**
Variance				**2.01**
Observations				**4**
df				**3**
t- test	**0.94**			
F	**2.49**			
t Critical two-tail	**2.45**			
F Critical one-tail	**9.28**			
Urine	**0.5**	**0.501**	**-0.20**	**100.20**
	1.2	**1.203**	**-0.25**	**100.25**
	1.7	**1.67**	**1.76**	**98.24**
	2.5	**2.54**	**-1.60**	**101.60**
Mean				**100.07**
Variance				**1.92**
Observations				**4**
df				**3**
t- test	**0.57**			
F	**2.59**			
t Critical two-tail	**2.45**			
F Critical one-tail	**9.28**			

Conclusion:

The present study describes the fabrication and validation of a novel disposable planner homemade disposable sensor integrated with ZnFR/MWCNTs nanocomposite for submicromolar voltammetric assaying of vanillylmandelic acid in biological samples. The electrode modifier showed high electrocatalytic activity against the oxidation of VMA molecule with improvement of the peak current compared with the unmodified sensors. At the optimum measuring conditions, calibration graphs were linear within the VMA concentration ranging from 0.11 to 2.74×10^{-6} mol L^{-1} with a LOD value of 0.03×10^{-6} mol L^{-1}. Indeed, the reported selectivity towards the VMA in the presence of various interfering species present in the urine samples introduced the fabricated sensors for analysis of the biological samples without prior pretreatment steps.

Acknowledgments

The authors express their great gratitude to the project fund received from the National Research Centre (NRC, Cairo, Egypt) for the internal grant (No. 13020205).

References:

1. G. Eisenhofer, I.J. Kopin, and D.S. Goldstein. Catecholamine metabolism: a contemporary view with implications for physiology and medicine. Pharmacol. Rev. 56 (3): 331 (2004).

2. M. Matsuo, R. Tasaki, H. Kodama, and Y. Hamasaki. Screening for Menkes disease using the urine HVA/VMA ratio. J. Inherited Metabolic Dis.: Official J. Soc. Study of Inborn Errors of Metabolism. 28(1):89 (2005).

3. T. Manickum. Simultaneous analysis of neuroendocrine tumor markers by HPLC-electrochemical detection. J. Chromatogr. B 877(32): 4140 (2009).

4. W.G. He, Y. Yan, W. Tang, R. Cai, and G. Ren. Clinical and biological features of neuroblastic tumors: a comparison of neuroblastoma and ganglioneuroblastoma. Oncotarget 8(23): 37730 (2017).

5. A. Garcıa, M. Heinänen, L.M. Jiménez, and C. Barbas. Direct measurement of homovanillic, vanillylmandelic and 5-hydroxyindoleacetic acids in urine by capillary electrophoresis. J. Chromatogr. A 871(1-2): 341 (2000).

6. M. Tuchman, C.L. Morris, M.L. Ramnaraine, L.D. Bowers, and W. Krivit. Value of random urinary homovanillic acid and vanillylmandelic acid levels in the diagnosis and management of patients with neuroblastoma: comparison with 24-hour urine collections. Pediatrics 75(2): 324 (1985).

7. S.A. Allen, S. Rednour, S. Shepard, and B.B. Pond. A simple and sensitive high-performance liquid chromatography–electrochemical detection assay for the quantitative determination of monoamines and respective metabolites in six discrete brain regions of mice. Biomed. Chromatogr. 31(11): e3998 (2017).

8. L. Mercolini, G. Gerra, M. Consorti, L. Somaini, and M.A. Raggi. Fast analysis of catecholamine metabolites MHPG and VMA in human plasma by HPLC with fluorescence detection and a novel SPE procedure. Talanta 78(1): 150 (2009).

9. K. Uchikura. Fluorometric determination of urinary vanilmandelic acid and homovanillic acid by high performance liquid chromatography after electrochemical oxidation. Anal. Sci. 6(3): 351 (1990).

10. M. Tsunoda. Recent advances in methods for the analysis of catecholamines and their metabolites. Anal. Bioanal. Chem. 386(3): 506 (2006).

11. G.M. Cao, and T. Hoshin. Simultaneous determination of 3, 4-dihydroxymandelic acid, 4-hydroxy-3-methoxymandelic acid, 3, 4-dihydroxyphenylglycol, 4-hydroxy-3-methoxyphenylglycol, and their precursors, in human urine by HPLC with electrochemical detection. Chromatographia, 47(7-8): 396 (1998).

12. R.T. Peaston, and C. Weinkove. Measurement of catecholamines and their metabolites. Ann. Clin. Biochem. 41(1): 17 (2004).

13. Y. Zhou, H. Yan, Q. Xie, S. Huang, J. Liu, Z. Li, A. Ma, S. Yao. Simultaneous analysis of dopamine and homovanillic acid by high-performance liquid chromatography with wall-jet/thin-layer electrochemical detection. Analyst 138(23); 7246 (2013).

14. J. Korf, and T. Valkenburgh-Sikkema. Fluorimetric determination of 5-hydroxyindoleacetic acid in human urine and cerebrospinal fluid. Clin. Chim. Acta 26(2): 301 (1969).

15. G. Fauler, H.J. Leis, E. Huber, C. Schellauf, R. Kerbl, C. Urban,and H. Gleispach. Determination of homovanillic acid and vanillylmandelic acid in neuroblastoma screening by stable isotope dilution GC-MS. J. Mass Spectrom. 32(5): 507 (1997).

16. M. Monteleone, A. Naccarato, G. Sindona, and A. Tagarelli. A reliable and simple method for the assay of neuroendocrine tumor markers in human urine by solid-phase microextraction–gas chromatography-triple quadrupole mass spectrometry. Anal. Chim. Acta, 759: 66 (2013).

17. G. Alemany, M. Akaarir, C. Rossello, and A. Gamundi. Thin-layer Chromatographic Determination of Catecholamines in Rat Plasma. Biomed. Chromatogr. 10(5): 225 (1996).

18. F. Taran, Y. Frobert, C. Créminon, J. Grassi, D. Olichon, C. Mioskowski, and P. Pradelles. Competitive enzyme immunoassay with monoclonal antibody for homovanillic acid measurement in human urine samples. Clin. Chem. 43(2): 363 (1997).

19. F. Taran, H. Bernard, A. Valleix, C. Créminon, J. Grassi, D. Olichon, J.R. Deverre, and P. Pradelles. Competitive enzyme immunoassay for urinary vanillylmandelic acid. Clin. Chim. Acta 264(2): 177 (1997).
20. J.J. Pisano, J.R. Crout, and D. Abraham. Determination of 3-methoxy-4-hydroxymandelic acid in urine. Clin. Chim. Acta 7(2): 285 (1962).
21. X. Li, W. Jin, and Q. Weng. Separation and determination of homovanillic acid and vanillylmandelic acid by capillary electrophoresis with electrochemical detection. Anal. Chim. Acta 461(1): 123 (2002).
22. D. Flottmann, J. Hins, C. Rettenmaier, N. Schnell, Z. Kuçi, G. Merkel, G Seitz, and G. Bruchelt. Two-dimensional isotachophoresis for the analysis of homovanillic acid and vanillylmandelic acid in urine for cancer therapy monitoring. Microchim. Acta 154(1): 49 (2006).
23. D. Barh, A. Carpi, M. Verma, and M. Gunduz (Eds.). Cancer biomarkers: minimal and noninvasive early diagnosis and prognosis. CRC Press (2014).
24. M.R. Siddiqui, Z.A. AlOthman, and N. Rahman. Analytical techniques in pharmaceutical analysis: A review. Arabian Journal of chemistry, 10, S1409-S1421 (2017).
25. S. Kurbanoglu, S.A. Ozkan, and A. Merkoçi. Electrochemical Nanobiosensors in Pharmaceutical Analysis. Novel Developments Pharm. Biomed. Anal. 2:302-353 (2018).
26. S.A. Ozkan, J.M. Kauffmann, and P. Zuman. Electroanalysis in biomedical and pharmaceutical sciences: voltammetry, amperometry, biosensors, applications. Springer (2015).
27. L. Angnes. Pharmaceuticals and personal care products. In Environmental analysis by electrochemical sensors and biosensors (pp. 881-903). Springer, New York, NY (2015).
28. A. Makrlikova, J. Barek, V. Vyskocil, and T. Navratil. Electrochemical methods for the determination of homovanillic, vanillylmandelic, and 5-hydroxy-3-indoleacetic acid as cancer biomarkers. Chem. Listy 112(9): 605 (2018).
29. R. Pfeifer, P.T. Martinhon, C. Sousa, J.C. Moreira, M.A.C. Nascimento, J. Barek, and V. Vyskočil. The role of 3, 4-dihydroxyphenylacetic acid adsorption in the oxidation of homovanillic acid at a glassy carbon rotating disc electrode. J. Electroanal. Chem. 838: 129 (2019).
30. S. Hafizi, Z.L. Kruk, and J.A. Stamford. Fast cyclic voltammetry: measurement of dopamine in the presence of its biological precursors and metabolites. J. Electroanal. Chem. 283(1-2): 125 (1990).
31. M.H. Joseph, H. Hodges, and J.A. Gray. Lever pressing for food reward and in vivo voltammetry: Evidence for increases in extracellular homovanillic acid, the dopamine metabolite, and uric acid in the rat caudate nucleus. Neurosci. 32(1): 195 (1989).
32. M.H. Joseph, and A.M. Young. Pharmacological evidence, using in vivo dialysis, that substances additional to ascorbic acid, uric acid and homovanillic acid contribute to the voltammetric signals obtained in unrestrained rats from chronically implanted carbon paste electrodes. J. Neurosci. Meth. 36(2-3): 209 (1991).
33. I.A. Mulla, J.P. Lowry, P.A. Serra, and R.D. O'Neill. Development of a voltammetric technique for monitoring brain dopamine metabolism: compensation for interference caused by DOPAC electrogenerated during homovanillic acid detection. Analyst 134(5): 893 (2009).
34. H. Dejmkova, H. Adamkova, J. Barek, and J. Zima. Voltammetric and amperometric determination of selected catecholamine metabolites using glassy carbon paste electrode. Monatsh. Chem.-Chem. Month. 148(3): 511 (2017).
35. M. Libansky, J. Zima, J. Barek, and H. Dejmkova. Voltammetric determination of homovanillic acid and vanillylmandelic acid on a disposable electrochemical measuring cell system with integrated carbon composite film electrodes. Monatsh. Chem.-Chem. Month 147(1): 89 (2016).
36. A. Makrlíková, E. Ktena, A. Economou, J. Fischer, T. Navrátil, J. Barek, and V. Vyskočil. Voltammetric determination of tumor biomarkers for neuroblastoma (homovanillic acid, vanillylmandelic acid, and 5-hydroxyindole-3-acetic acid) at screen-printed carbon electrodes. Electroanal. 29(1): 146-153 (2017).
37. B. Fu, H. Chen, Z. Yan, Z. Zhang, J. Chen, T. Liu, and K. Li. A simple ultrasensitive electrochemical sensor for simultaneous determination of homovanillic acid and vanillylmandelic acid in human urine based on MWCNTs-Pt nanoparticles as peroxidase mimics. J. Electroanal. Chem. 866: 114165 (2020).
38. Y. Ruan, P. Shi, Y. Lei, S. Weng, S. Li, L. Huang, X. Lin, and H. Yao. Polyvinyl butyral/graphene oxide nanocomposite modified electrode for the integrate determination of terminal metabolites of catecholamines in human urine. J. Electroanal. Chem. 848: 113267 (2019).
39. A. Hatefi-Mehrjardi, N. Ghaemi, M.A. Karimi, M. Ghasemi, and S. Islami-Ramchahi. Poly-(alizarin red s)-modified glassy carbon electrode for simultaneous electrochemical determination of levodopa, homovanillic acid and ascorbic acid. Electroanal. 26(11): 2491 (2014).
40. S. Baluchová, J. Barek, L.I. Tomé, C.M. Brett, and K. Schwarzová-Pecková. Vanillylmandelic and homovanillic acid: Electroanalysis at non-modified and polymer-modified carbon-based electrodes. J. Electroanal. Chem. 821: 22 (2018).

41. T.V. Shishkanova, G. Broncová, P. Fitl, V. Král, and J. Barek. Voltammetric detection of catecholamine metabolites using Tröger's base modified electrode. Electroanal. 30(4): 734 (2018).
42. R. El Khamlichi, D. Bouchta, M.B. Atia, A. Attar, M. Choukairi, S. Tazi, R. Ihssane, C. Faiza, D. Khalid, and R.T. Khalid. A novel L-leucine modified sol-gel-carbon electrode for simultaneous electrochemical detection of homovanillic acid, dopamine and uric acid in neuroblastoma diagnosis. Mater. Sci. Eng. C, 71: 870-878 (2017).
43. M.C. Blanco-López, M.J. Lobo-Castañón, A.J.M. Ordieres, and P. Tuñón-Blanco. Electrochemical behavior of catecholamines and related compounds at in situ surfactant modified carbon paste electrodes. Electroanal. 19(2-3): 207 (2007).
44. K.A. Al-Ola, A.A Alfi, A. Hameed, A.M. Munshi, Z.A. Al-Ahmed, A.A., Keshk, M.E. Khalifa, and N.M. and El-Metwaly. Zinc Ferrite nanostructure/multi-walled carbon nanotubes (ZFO/MWCNTs) nanocomposite as sensor for homovanillic acid detection in urine samples for cancer therapy monitoring. International Journal of Electrochemical Science, 16(8), p.210838 (2021).
45. H.A. Abbas, A.L.A. Radwan, E. Khaled, and R.Y. Hassan. Synthesis and characterization of nanostructured copper and lanthanum co-doped zirconia for voltammetric sensing of tumor biomarkers. Electrochemical Science Advances, 2(5), p.e2100109 (2022).
46. M.A Maksoud, G.S El-Sayyad, A.H. Ashour, A.I. El-Batal, M.S. Abd-Elmonem, H.A. Hendawy, E.K. Abdel-Khalek, S. Labib, E. Abdeltwab, and M.M. El-Okr. Synthesis and characterization of metals-substituted cobalt ferrite [Mx Co (1-x) Fe2O4;(M= Zn, Cu and Mn; x= 0 and 0.5)] nanoparticles as antimicrobial agents and sensors for Anagrelide determination in biological samples. Mater. Sci. Eng. C, 92: 644 (2018)
47. T. Tatarchuk, M. Bououdina, W. Macyk, O. Shyichuk, N. Paliychuk, I. Yaremiy, B. Al-Najar B, and M. Pacia. Structural, optical, and magnetic properties of Zn-doped CoFe 2 O 4 nanoparticles. Nanoscale Res. Lett. 12(1): 1 (2017).
48. S.B. Mullani, A.G. Dhodamani, A. Shellikeri, N.B. Mullani, A.K. Tawade, S.N. Tayade, J. Biscay, L. Dennany, and S.D. Delekar. Structural refinement and electrochemical properties of one dimensional (ZnO NRs) 1− x (CNs) x functional hybrids for serotonin sensing studies. Sci. Rep. 10(1): 1 (2020).
49. S.B. Khan, S. Irfan, and S.L. Lee. Influence of Zn+ 2 Doping on Ni-Based Nanoferrites;(Ni1− x ZnxFe2O4). Nanomaterials, 9(7): 1024 (2019)
50. Guideline, ICH Harmonised Tripartite. "Validation of analytical procedures: text and methodology." Q2 (R1) 1, no. 20 (2005): 05
51. V. Jouikov, and J. Simonet. Electrochemical reactions of sulfur organic compounds. Encyclopedia of electrochemistry, Vol. 8. Weinheim, Germany: Wiley-VCH Verlag GmbH and Co.; 2007. pp. 235e71 (V. Jouikov, and J. Simonet). Electrochemical reactions of sulfur organic compounds. Encyclopedia of Electrochemistry: Online (2007).
52. A.K. Vidyadharan, J. Divya, and T.E. Mary. Ni0.1Co0.9 Fe2O4-based electrochemical sensor for the detection of paracetamol. J. Solid State Electrochem. 18 (9): 2513 (2014).
53. Z. Shahnavaz, L. Farnaz, P.M. Woi, and A. Yatimah. Core-shell–CuFe2O4/PPy nanocomposite enzyme-free sensor for detection of glucose. J. Solid State Electrochem. 19 (4): 1223 (2015).
54. J. Jaime-González, E. Mazario, N. Menendez, J. Sanchez-Marcos, A. Muñoz-Bonilla, and P. Herrasti. Comparison of ferrite nanoparticles obtained electrochemically for catalytical reduction of hydrogen peroxide. J. Solid State Electrochem. 20 (4): 1191 (2016).
55. J. Bicker, A. Fortuna, G. Alves, and A. Falcao. Liquid chromatographic methods for the quantification of catecholamines and their metabolites in several biological samples—A review. Anal. Chim. Acta 768: 12 (2013).
56. N. Elgrishi, K.J. Rountree, MB.D. Carthy, E.S. Rountree, T.T. Eisenhart, and J.L. Dempsey. A practical beginner's guide to cyclic voltammetry. J. Chem. Educ. 95(2): 197 (2018).
57. Z. Zhang, and E. Wang. Electrochemical principles and methods, Science Press, Beijing (2000).
58. D.K. Gosser. Cyclic voltammetry, simulation and analysis of reaction mechanisms, Wiley VCH, New York, (1993).
59. E. Laviron,. Theoretical study of a reversible reaction followed by a chemical reaction in thin layer linear potential sweep voltammetry. J. Electroanal. Chem. Interf. Electrochem. 39, 1-23 (1972)
60. Al-Nami, S.Y., Azher, O.A., Aljuhani, E., Shah, R., Al-Qahtani, S.D., Khalifa, M.E. and El-Metwaly, N.M., 2021. Voltammetric behavior of acidic catecholamine metabolites in presence of cationic surfactants. Journal of The Electrochemical Society, 168(10), p.106507